Check for updates

Comonomer effects in vinyl based photocatalytic polymers†

Thomas Kuckhoff,‡[a] Julian Heuer,‡[a] Rong Li,[a] Kai A. I. Zhang, [ID] §[a] Katharina Landfester [ID] *[a] and Calum T. J. Ferguson [ID] *[a,b]

The copolymerization of photocatalytic moieties into a polymeric material has emerged as a new development platform for heterogeneous photocatalysts. Incorporating small molecule photocatalysts into polymeric structures has created a new class of heterogeneous photocatalysts. However, the effect and interaction of the comonomer on the photocatalyst have been mostly ignored and little is known about the influence of classical polymer composition on photocatalytic efficiency. Here a vinyl functionalized benzothiadiazole photocatalyst was copolymerized with three dramatically different monomers, methyl methacrylate, styrene, and acrylonitrile, *via* free radical polymerization, to investigate the effect of the comonomer choice on the photophysical properties and photocatalytic efficiency.

Photocatalysis uses visible light to facilitate chemical reactions and can remove the need for thermal energy, establishing itself as a more environmentally friendly alternative to classic catalysis.[1–3] Rapid development over the last decade has provided access to a wide range of reactions previously only achieved through the use of classic catalysts.[4–10] However, homogeneous and heterogeneous photocatalysts suffer from significant intrinsic drawbacks,[11–15] including photobleaching, a lack of easy recycling possibilities, limited mass transport to the active center, or poor light absorption.[16–20]

An ideal photocatalyst would possess the benefits of both homogeneous and heterogeneous systems, achieving high efficiency while allowing the alteration of materials properties.[21] Therefore, the fixation of photocatalytic moieties onto support materials has been recently investigated by com-

bining the photocatalytic properties of small molecule homogeneous photocatalysts with the material properties of the support. This creates a wide range of possible photocatalytic structures where materials properties can be easily adjusted. One of the easiest and most efficient ways to incorporate single photocatalytic moieties into the support material is their copolymerization *via* free or controlled radical polymerization.[22,23] Polymers are an ideal platform as support materials possessing a variety of classic monomers giving control over materials properties and structural designs including hydrogels, microgels and responsive nanoparticles.[24] Interestingly, while it is well known that the structural design and solvents can directly influence the photocatalytic efficiency, the monomer used in the copolymerization is chosen due to the desired material properties of the polymer. The interaction between the photocatalyst and the comonomer is often overseen, however, assuming negligible interaction between the photocatalyst and surrounding polymer minimal influences on the photocatalytic efficiency might be observed.

Kobayashi and Yoo reported the copolymerization of an iridium photocatalyst into three heterogeneous polymers. Based on the used combination of ethyl methacrylate and styrene, *N*-isopropyl acrylamide, or benzyl methacrylate, different photocatalytic efficiencies were observed.[25] Additionally, we have recently reported the copolymerization of a benzothiadiazole-based photocatalyst into a self-assembled diblock copolymer. Depending on the position of the photocatalytic unit in the hydrophobic core or the hydrophilic corona, differences in photocatalytic efficiency could be observed.[26] Similar effects are reported in the emerging field of artificial photoenzymes, where the microenvironment of the protein scaffold can affect the photocatalytic efficiency depending on the placement of the photocatalytic moiety (Fig. 1).[27]

A systematic study is needed to investigate the effects of the electron-withdrawing groups, steric hindrance, and charge density of the comonomer on photocatalytic performance. In this study, three commonly used monomers, styrene (S), methyl methacrylate (MMA), and acrylonitrile (AN), were

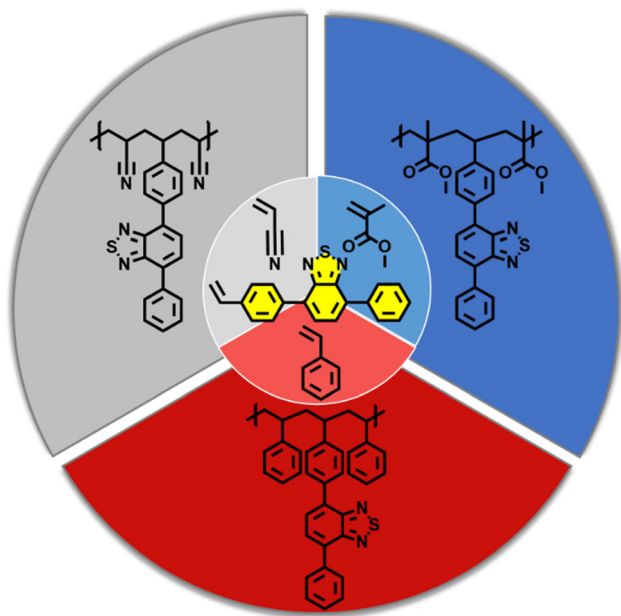[a]*Max Planck Institute for Polymer Research, Ackermannweg 10, 55128 Mainz, Germany*
[b]*School of Chemistry, University of Birmingham, Edgbaston, Birmingham, B15 2TT, UK. E-mail: c.ferguson.1@bham.ac.uk*

‡These authors contributed equally to this work.

§Unfortunately, Prof Kai Zhang passed away during the completion of this manuscript.

Fig. 1 A photocatalytic moiety is copolymerized with three distinct monomers, styrene, methyl methacrylate and acrylonitrile, to investigate the effect of the comonomer on the photocatalytic efficiency and photophysical properties.

copolymerized with a metal-free organic photocatalytic moiety to analyze the comonomer effect on the photocatalytic behavior. The resulting copolymers were fully characterised by gel permeation chromatography (GPC), infrared (IR), UV/Vis-absorbance, fluorescence lifetime, quantum yield, and dynamic light scattering (DLS) measurements. In addition, density-functional theory (DFT) and Tauc-plot calculations and cyclic voltammetry were used to determine the HOMO/LUMO levels and the resulting bandgap. Finally, the photocatalytic efficiency was investigated *via* kinetic studies of three model reactions, revealing significant discrepancies in the performance based on the chosen comonomer.

Results and discussion

One of the simplest donor–acceptor photocatalysts contains a benzothiadiazole unit as an electron acceptor and two phenyl groups as electron donors. As this photocatalyst contains few functional groups the possibility of interference with the polymer or substrate is limited. This makes it an ideal candidate for investigating the possible influence of the surrounding polymer microenvironment. This photocatalyst was modified with vinyl functionalization to allow easy copolymerization. The functional group was chosen to replicate the unmodified homogeneous photocatalyst incorporated into a polymer backbone while preventing changes in the optical properties and photocatalytic activity.

Three different monomers (styrene, methyl methacrylate, and acrylonitrile) with varying polarities, dielectric constants,

and possible interactions with the photocatalyst were investigated. The aromatic nature of polystyrene could enable possible π–π-interactions between the photocatalyst and the polymer backbone.[28,29] Additionally, due to its highly polar backbone, beneficial charge stabilization could be observed for polyacrylonitrile, affecting the efficiency of the photocatalyst.[30,31]

From our previous experience, a photocatalytic (BT) loading of 5 wt% was selected as this gives good photocatalyst performance while maximizing the possible comonomer influence. Three distinct copolymers are based on polystyrene (PS-BT), poly(methyl methacrylate) (PMMA-BT), and polyacrylonitrile (PAN-BT). The copolymers were analyzed, and the incorporation of photocatalysts was confirmed by GPC, ^{1}H NMR, UV/Vis, and FTIR. The copolymers possessed molecular weights between 15 000 and 20 000 g mol^{-1} and dispersities of 2.4–3Đ (Fig. S12†). All three polymers readily dissolve in dimethylformamide (DMF) and it was therefore chosen as the solvent system for photocatalytic testing. As the polymer's swelling behavior and structure could impact the photocatalytic efficiency, the hydrodynamic radii were determined. The copolymers have comparable hydrodynamic radii between 6 and 8 nm, allowing a direct comparison of the photocatalytic efficiency (Fig. S10†).

FTIR allowed easy identification of the polymers showing specific bands at 1700–1800 cm^{-1} and 700 cm^{-1} for aromatic –C–H bending in PS-BT, at 2250 cm^{-1} for C≡N stretching in PAN-BT and at 1700 cm^{-1} for ester-C=O stretching in PMMA-BT (Fig. S11†). As previously reported, the low concentration of the incorporated photocatalyst makes quantification and detection by FTIR difficult. Even with higher weight percentages of photocatalysts, the IR-bands at 700 cm^{-1} are the only indication of incorporation.

^{1}H-NMR analysis highlights the photocatalytic moiety between 8.3 and 7 ppm for PMMA-BT and PAN-BT, while in the case of PS-BT the styrene signal overlaps partly with that of the photocatalytic moiety. The polymer backbone can be observed at 2.4–1.9 and 3.6–3.1 ppm for PAN-BT, 3.8–3.3, 2.0–1.7 and 1.1–0.5 ppm for PMMA-BT, and 7.3–6.2 and 2.4–1.0 ppm for PS-BT (Fig. S23–25†). The incorporation of the photocatalyst was determined *via* UV/Vis-absorbance measurements (Fig. S1†).

The solvent affects the UV/Vis absorbance spectrum of the non-functionalized homogeneous photocatalyst 4,7-diphenyl-benzo-[2,1,3]thiadiazole (Ph-Bt-Ph), displaying a hypsochromic shift depending on the solvent, shifting from 392 in toluene to 384 nm in acetonitrile (Table 1 and Fig. S1†), indicating the stabilization of a slightly more polarized ground state. This effect can be observed and replicated in polymers. Incorporation of the photocatalyst into a polymer backbone resulted in comonomer-dependant shifts in the absorbance spectra. In PMMA-BT and PS-BT, the main absorbance peak does not shift significantly (392 and 390 nm, respectively), while in PAN-BT, the peak blue-shifted by 7 nm (385 nm; Table 1). These values are similar to those of the homogeneous photocatalyst in toluene and ACN, respectively, showcasing

Table 1 Measured and calculated values for PMMA-BT, PAN-BT and PAN-BT. Absorbance, emission, excitation maxima and fluorescence lifetime were measured in DMF. Quantum yield was measured in DMF against 4,7-diphenyl-2,1,3-benzothiadiazole in ACN at 366 nm. DFT calculations were performed using B3LYP 6-31+g(d). Optical bandgap calculations were based on UV/Vis-measurements in DMF

| Entry	Polymer	Absorbance peak (nm)	Emission peak (nm)	Excitation (nm)	$\Phi_{polymer}/\Phi_{photocatalyst}$	τ_o (ns)	$E_{g\ opt}$ (eV)	HOMO/LUMO(DFT) V vs. SCE
1	PMMA-BT	390	507	383	1.01	11.0	2.87	1.52/−1.78
2	PS-BT	392	509	385	1.00	11.1	2.89	1.52/−1.77
3	PAN-BT	386.5	503	379	0.82	10.2	2.92	1.80/−1.55

that the immediate environment of the polymer has an impact on the stabilization of the catalyst, similar to a change in the solvent. PAN is a highly polar polymer with high dielectric values leading to a blue shift compared to PS. Similar trends can be observed in the emission and excitation spectra. The emission and excitation peaks indicate a similar blue shift, with PS-BT having the highest emission peak at 509 nm followed by PMMA-BT at 507 nm and PAN-BT at 503 nm, with all three copolymers possessing the same Stokes shift of 117 nm (Table 1 and Fig. S4†).

The fluorescence lifetimes of all three polymers were between 10 and 11 ns, with PS-BT having the highest and PAN-BT having the lowest fluorescence lifetime (Fig. S7†). The lifetime measurements for PS-BT and PMMA-BT show negligible differences of 11.1 and 11.0 ns. In comparison, the lifetime of the excited state of the photocatalytic moiety in PAN-BT is reduced to 10.2 ns. The lifetime of the photogenerated species is typically directly related to photocatalytic efficiency, so we would expect PAN-BT to underperform.

The quantum yield of the unmodified 4,7-diphenyl-2,1,3-benzothiadiazole ($\Phi_{photocatalyst}$ 80) measured against quinine sulfate (1 M H_2SO_4) was previously reported by DaSilveira Neto.[32,33] We investigated if the quantum yield of the photocatalytic unit was again influenced by the microenvironment. PS-BT and PMMA-BT again only showed minor differences and a comparable high quantum yield to the unmodified 4,7-diphenyl-2,1,3-benzothiadiazole (Table 1 and Fig. S6†). PAN-BT, on the other hand, showed a much lower quantum yield of 0.82 compared to the free photocatalyst. This difference may be due to the increasing absorbance of the polymer backbone at a lower wavelength, leading to non-radiant relaxation playing a more prominent role in PAN-BT. This significant decrease in quantum yield has a negative impact on the photocatalytic performance.

The band gap and energy of the orbitals are crucial for the photocatalytic performance and determine the reductive and oxidative capabilities of the photocatalyst. Through copolymerization, Huber *et al.* incorporated a benzothiadiazole photocatalyst in a heterogeneous organogel based on crosslinked PMMA. Through cyclic voltammetry and DFT calculations of the pure photocatalyst and the copolymer, changes in the bandgap, as well as the HOMO and LUMO levels, could be observed.[34] Therefore, the HOMO/LUMO levels of the copolymers and the band gap were calculated and analyzed using DFT calculations, cyclic voltammetry, and Tauc-plots.

The theoretical orbital energies were determined for trimers using B3LYP[35,36] with the basis set 6-31+g(d).[37,38] Depending on the comonomer, the calculation indicates different values for the HOMO/LUMO levels for PS-BT, PAN-BT, and PMMA-BT (Fig. 2B). PS-BT and PMMA-BT show only minor differences in the band gap at 3.29 and 3.30 eV. The LUMO and HOMO levels for both PS and PMMA polymers are the same at −1.37 V *vs.* SCE (LUMO) and 1.92 V *vs.* SCE for the HOMO, respectively. Conversely, PAN showed the largest elec-
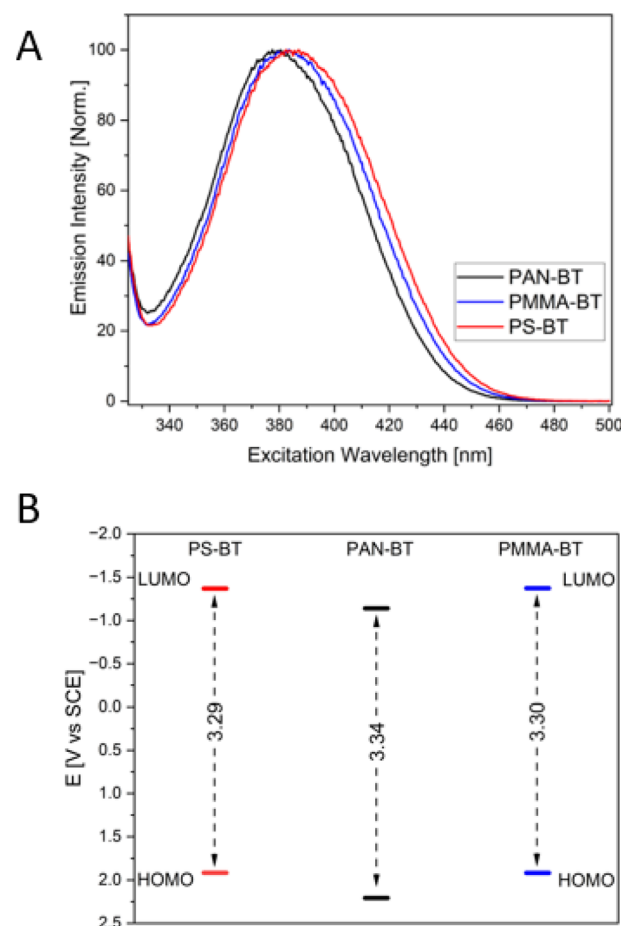
Fig. 2 Three copolymers were analyzed *via* (A) excitation spectra and (B) DFT calculations. (A) The copolymers show a blue shift from styrene to the polar acrylonitrile comonomer. (B) DFT calculations confirm a higher bandgap for PAN-BT, while PMMA-BT and PS-BT lay closer together.

© 2024 The Author(s). Published by the Royal Society of Chemistry

RSC Appl. Polym., 2024, **2**, 155–162 | **157**

tron gap at 3.34 V *vs.* SCE and the lowest LUMO and highest HOMO level energies with $-1.14/2.21$ V *vs.* SCE.

Cyclic voltammetry measurements indicated only small differences between the polymers and are smaller compared to the theoretical values. The reduction onset was determined to be -1.35 V *vs.* SCE for PMMA-BT, -1.3 for PS-BT and -1.29 for PAN-BT (Fig. S13†). These values are comparable to previous cyclic voltammetry measurements of PMMA and poly(*N,N*-dimethylacrylamide) with a copolymerized benzothiadiazole based photocatalyst.[39,40]

In addition to DFT calculations and CV measurements, the average optical electron bandgap was determined[41,42] (Table 1 and Fig. S3†). The values were used to determine the HOMO levels of all polymers. The values are smaller than those predicted by the DFT calculations, at around 2.9 eV. It can be observed again that PAN-BT has a larger electron gap (2.92 eV) compared to PS-BT (2.89 eV) and PMMA-BT (2.87 eV).

A clear effect of the comonomer on the molecular orbital energies of the photocatalytic unit was observed. Interestingly, no real differences between St and MMA based polymers were observed, showing that the π-interactions do not have much of an influence. Conversely, a significant difference was observed with the AN based polymer, where the polar nature of the comonomer significantly blue shifted the photocatalyst.

After observing changes in optical properties and bandgaps depending on the chosen comonomer we decided to further investigate the comonomer influence on the photocatalytic efficiency through kinetic studies of three model reactions. Further Stern–Volmer plots were used to investigate the interaction between sacrificial agents and the copolymers.[43] The model reactions were chosen to include the hydroxylation of boronic acids, the C–C coupling of benzyl bromide and an electron-rich heterocyclic indole coupling reaction. The photocatalytic reaction covers a variety of conditions under nitrogen and oxygen, and the usage of different sacrificing agents. First, the hydroxylation of diphenyl boronic acid was investigated. This reaction is well established and various publications cover its mechanistic investigations, possible conditions, and usable photocatalysts.[44] The reaction was conducted with all three copolymers under blue light irradiation at room temperature. The copolymers successfully catalysed the hydroxylation, leading to high conversion in all three cases (Fig. 3). The kinetic study was analysed over a time span of 6 hours, reaching over 90% conversion for PS-BT, PMMA-BT and PAN-BT. PAN-BT showed the lowest conversion of 90%. Nevertheless, all three polymers reach high turnover numbers of 900–960. Interestingly, the kinetic study indicates that PS-BT has a higher conversion rate reaching 87% after 4 h compared to 74% and 82% for PAN-BT and PMMA-BT, showcasing a slightly higher efficiency for PS-BT over PMMA-BT or PAN-BT.

Mechanistic investigations by Pitre *et al.* highlighted the necessity of a superoxide for the hydroxylation of boronic acids.[45] Therefore, the reaction was conducted under an oxygen atmosphere in DMF in the presence of DIPEA as a sacrificing agent. The role of the sacrificing agent was investigated through Stern–Volmer plots (Fig. S8/9†), indicating a
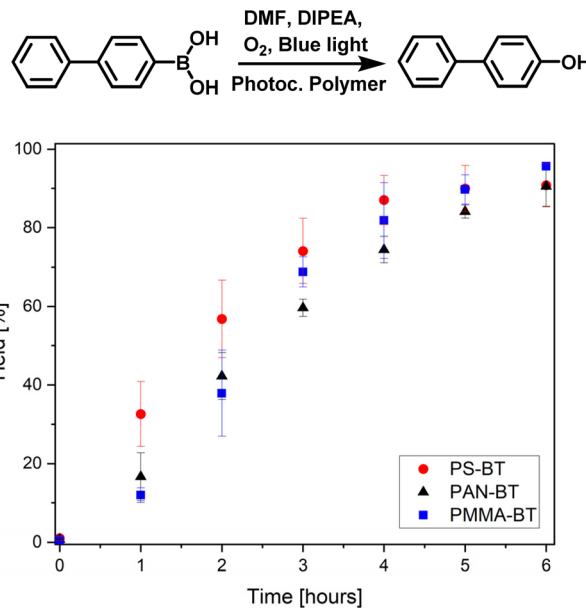

Fig. 3 Photocatalytic hydroxylation of 4-biphenyl boronic acid measured over time using PS-BT, PMMA-BT and PAN-BT, calibrated against 1-bromooctane (Fig. S15†) 4-biphenylboronic acid (19.8 mg, 100 μmol) *N,N*-diisopropylethylamine (52 μL, 300 μmol) and photocatalytic polymer (100 nmol photoactive unit) in DMF (2 mL), under an O_2 atmosphere with blue light irradiation.

similar quenching rate for all three polymers. Here, an electron is transferred from the photocatalyst to oxygen, which then interacts with the substrate. Oxygen can quickly diffuse into the swollen photocatalytic polymer. Therefore, the chemistry of the polymer only has a limited effect on the reactivity. The PS based photocatalyst performed slightly better than the other systems, and this may be due to the higher affinity of the aromatic substrate to the polymer increasing the proximity of the photogenerated radicals to the substrate (Fig. 4).

As a second photocatalytic reaction, the C–C coupling reaction of 4-chlorobenzylbromide was investigated, which was previously not reported for this photocatalyst (Fig. 2).[46] Li *et al.* reported the usage of a Cu-modified TiO_2 photocatalyst for the C–C coupling under UV-irradiation.[47] Here, the reaction was performed under blue light irradiation in the presence of DIPEA. The coupling again indicates a comonomer effect on the efficiency of the photocatalytic moiety. The photocatalytic reaction was analysed *via* a kinetic study over a time span of eight hours in which a conversion of 61 to 83% was achieved. The highest conversion of 83% and a TON of 277 were again yielded by PS-BT, followed by PAN-BT and PMMA-BT with 68 and 61% conversion and TON values of 227 and 203, respectively. Interestingly, the reaction was first attempted with triphenylamine (TPA) instead of DIPEA to prevent hydrogen transfer and the formation of 4-chlorobenzylbromide as a side product. Interestingly, the reaction showed a slower reaction rate in the presence of TPA. Nevertheless, it was observed that the formation of 4-chlorotoluene is also disfavoured in the presence of DIPEA, and only traces of 4-chlorotoluene were
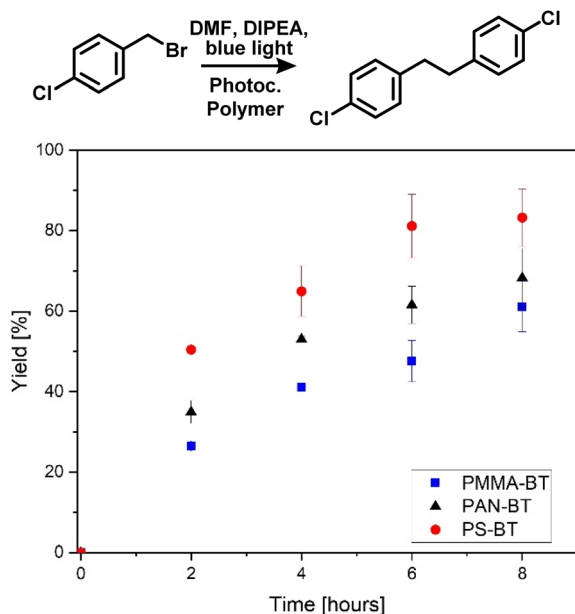
Fig. 4 Photocatalytic C−C coupling of 4-chlorobenzylbromide over eight hours using Ps-BT, PMMA-BT and PAN-BT, indicating a comonomer effect on the overall efficiency, calibrated against 1-bromooctane (Fig. S16†) 4-chlorobenzyl bromide (20.5 mg, 100 μmol) N,N-diisopropylethylamine (175 μL, 1 mmol) and photocatalytic polymer (300 nmol photocatalytic moiety) in DMF (2 mL), under a N_2 atmosphere with blue light irradiation.

observed (Fig. S15†). This reaction requires a close proximity between the photocatalyst and substrate as it proceeds using the photoexcited electron. As PS-BT had the longest lifetime and highest absorbance wavelength it outperformed the other photocatalytic polymers.

Finally, the C−C coupling between diethyl bromomalonate and 3-methyl indole was investigated (Fig. 5). The reaction was performed quickly within 90 min, requiring the usage of TPA to reduce the favored dehalogenation of diethyl bromomalonate. GCMS analysis, in combination with a kinetic study, highlights the total conversion of the indole to the desired product (Fig. S17†). Using PS-BT, a complete conversion of the indole is observed in 80 min (600 TON). PMMA-BT, in comparison, reaches a TON of 360 in 80 min, indicating a 40% decrease in efficiency. Lastly, PAN-BT again shows the lowest photocatalytic efficiency reaching a conversion of 20% (120 TON) which highlights the most significant drop in performance under all tested reactions. Although the contrast in the capability of the copolymers is significant, the trend is comparable to that of the previous reaction, where PS-BT outperformed PMMA-BT or PAN-BT. Furthermore, the quenching behavior of TPA was analyzed, showing quenching results and a decrease in fluorescence comparable to those of DIPEA. The general trend is repeated, with all three copolymers showing only slight variations and PAN-BT being slightly elevated compared to PS-BT and PMMA-BT (Fig. S8/9†).

Interestingly, differences in photocatalytic activity were again observed between PS-BT and PMMA-BT which have very
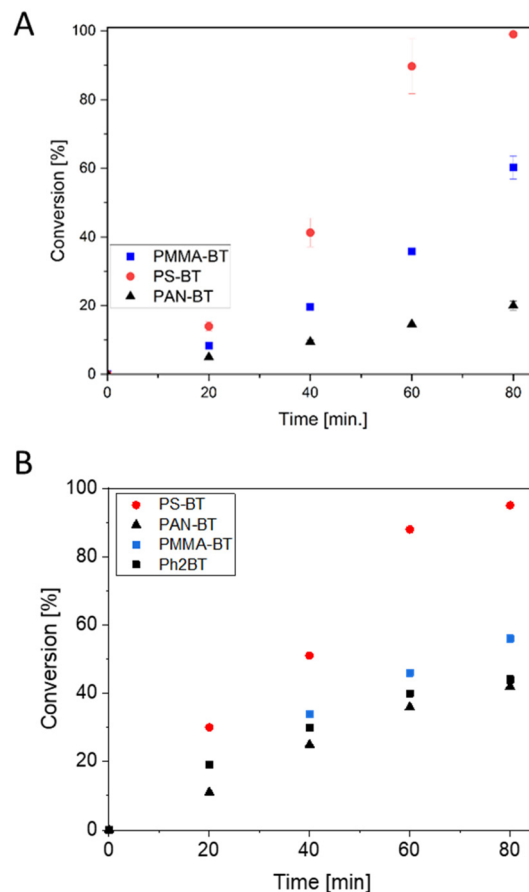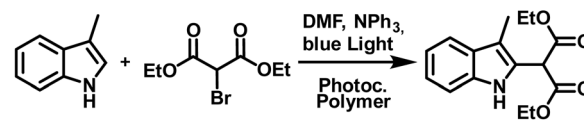
Fig. 5 (A) Kinetic investigation of the C−C coupling of 3-methyl indole using a 5% photocatalyst containing polymer. Measurements were carried out over 80 minutes showing full conversion for PS-BT. 3-Methyl indole (19.7 mg, 150 μmol), diethyl bromomalonate (71.7 mg, 300 μmol), triphenylamine (73.6 mg, 300 μmol) and photocatalytic polymer (5% polymer, 250 nmol photoactive unit) in DMF (2 mL) under an Ar atmosphere with blue light irradiation were used. (B) Kinetic investigation of the C−C coupling of 3-methyl indole using a 1% photocatalyst containing polymer or small molecule. Measurements were carried out over 80 minutes showing full conversion for PS-BT. 3-Methyl indole (19.7 mg, 150 μmol), diethyl bromomalonate (71.7 mg, 300 μmol), triphenylamine (73.6 mg, 300 μmol) and photocatalytic polymer (5% polymer, 250 nmol photoactive unit) in DMF (2 mL) under an Ar atmosphere with blue light irradiation were used.

similar photophysical properties. This suggests that another factor influences the photocatalytic efficency, which may be due to the affinity of the substrate to the polymer which we have previously demonstrated to affect the rate of conversion.

The effect of photocatalyst concentration was investigated by synthesising a polymer containing 1% of the photocatalyst. When we kept the concentration of the photocatalytic unit constant in the reaction media a similar conversion for the C−C

© 2024 The Author(s). Published by the Royal Society of Chemistry

RSC Appl. Polym., 2024, **2**, 155–162 | **159**

coupling of 3-methyl indole was observed (Fig. 5B). As a further comparison we undertook the reaction with the analogous small molecule photocatalyst PH$_2$BT. Here, the small molecule performed similarly to both the PMMA and PAN based photocatalysts but was outperformed by the PS based system (Fig. 5B). This again suggests that mass transport of the substrate to the photocatalytic center could be crucial in efficient photocatalytic performance, where the aromatic polymer creates a higher local concentration of the aromatic substrate, increasing the conversion rate.

Conclusion

In summary, we copolymerized three common monomers with a donor–acceptor-based photocatalyst and investigated the impact of the comonomer on the photocatalytic activity. In a first step the photophysical properties were investigated. While the differences between PMMA-BT and PS-BT are negligible, PAN-BT shows deviating values, indicating a lower lifetime of the excited state as well as a reduced quantum yield and a blue shift of the absorption and emission spectra.

In the next step, the photocatalytic performance of the three copolymers where analyzed in three kinetic studies, and the conversion and TON were determined. Through this catalytic testing, it could be shown that the comonomer choice impacts the photocatalytic efficiency. The hydroxylation of boronic acids was not significantly impacted by the comonomer choice, which may be due to the oxygen diffusion into the material not being hindered or enhanced in any structure. In C–C coupling reactions, a closer proximity between the photocatalyst and the substrate is needed, and more significant differences are observed.

Interestingly, an overall trend in photocatalytic performance was observed, which was similar to the measured optical properties. PS-BT possessed the highest absorbance wavelength paired with the longest lifetime of the excited state and could outperform the other two copolymers. On the other hand, PAN-BT showed a higher blue shift and a lower lifetime, leading to a lower performance under visible light irradiation. Further investigation needs to be undertaken to look at what apart from the photophysical properties of a photocatalytic materials can affect the reaction rate.

Our results indicate that depending on the photocatalytic reaction, the chosen polymer can impact the performance, and an adequate and suitable copolymer must be chosen.

Conflicts of interest

There are no conflicts to declare.

References

1 C. Rosso, G. Filippini, A. Criado, M. Melchionna, P. Fornasiero and M. Prato, Metal-Free Photocatalysis: Two-Dimensional Nanomaterial Connection toward Advanced Organic Synthesis, *ACS Nano*, 2021, **15**(3), 3621–3630, DOI: **10.1021/acsnano.1c00627**.

2 Y. Zhi, Z. Wang, H. L. Zhang and Q. Zhang, Recent Progress in Metal-Free Covalent Organic Frameworks as Heterogeneous Catalysts, *Small*, 2020, **16**(24), e2001070, DOI: **10.1002/smll.202001070**.

3 J. Heuer and C. T. J. Ferguson, Photocatalytic polymer nanomaterials for the production of high value compounds, *Nanoscale*, 2022, **14**(5), 1646–1652, DOI: **10.1039/d1nr06985c**.

4 M. J. Genzink, J. B. Kidd, W. B. Swords and T. P. Yoon, Chiral Photocatalyst Structures in Asymmetric Photochemical Synthesis, *Chem. Rev.*, 2022, **122**(2), 1654–1716, DOI: **10.1021/acs.chemrev.1c00467**.

5 L. Marzo, S. K. Pagire, O. Reiser and B. Konig, Visible-Light Photocatalysis: Does It Make a Difference in Organic Synthesis?, *Angew. Chem., Int. Ed.*, 2018, **57**(32), 10034–10072, DOI: **10.1002/anie.201709766**.

6 N. A. Romero and D. A. Nicewicz, Organic Photoredox Catalysis, *Chem. Rev.*, 2016, **116**(17), 10075–10166, DOI: **10.1021/acs.chemrev.6b00057**.

7 M. H. Shaw, J. Twilton and D. W. MacMillan, Photoredox Catalysis in Organic Chemistry, *J. Org. Chem.*, 2016, **81**(16), 6898–6926, DOI: **10.1021/acs.joc.6b01449**.

8 J. Twilton, C. Le, P. Zhang, M. H. Shaw, R. W. Evans and D. W. C. MacMillan, The merger of transition metal and photocatalysis, *Nat. Rev. Chem.*, 2017, **1**, 0052, DOI: **10.1038/s41570-017-0052**.

9 J. Xuan and W. J. Xiao, Visible-light photoredox catalysis, *Angew. Chem., Int. Ed.*, 2012, **51**(28), 6828–6838, DOI: **10.1002/anie.201200223**.

10 J. W. Tucker and C. R. J. Stephenson, Shining Light on Photoredox Catalysis: Theory and Synthetic Applications, *J. Org. Chem.*, 2012, **77**(4), 1617–1622, DOI: **10.1021/jo202538x**.

11 A. P. Demchenko, Photobleaching of organic fluorophores: quantitative characterization, mechanisms, protection, *Methods Appl. Fluoresc.*, 2020, **8**(2), 022001, DOI: **10.1088/2050-6120/ab7365**.

12 L. S. Herculano, L. C. Malacarne, V. S. Zanuto, G. V. B. Lukasievicz, O. A. Capeloto and N. G. C. Astrath, Investigation of the Photobleaching Process of Eosin Y in Aqueous Solution by Thermal Lens Spectroscopy, *J. Phys. Chem. B*, 2013, **117**(6), 1932–1937, DOI: **10.1021/jp3119296**.

13 H. Chen, H. S. Jena, X. Feng, K. Leus and P. Van Der Voort, Engineering Covalent Organic Frameworks as Heterogeneous Photocatalysts for Organic Transformations, *Angew. Chem., Int. Ed.*, 2022, **61**(47), e202204938, DOI: **10.1002/anie.202204938**.

14 R. Li, J. Byun, W. Huang, C. Ayed, L. Wang and K. A. I. Zhang, Poly(benzothiadiazoles) and Their Derivatives as Heterogeneous Photocatalysts for Visible-Light-Driven Chemical Transformations, *ACS Catal.*, 2018, **8**(6), 4735–4750, DOI: **10.1021/acscatal.8b00407**.

15 T.-X. Wang, H.-P. Liang, D. A. Anito, X. Ding and B.-H. Han, Emerging applications of porous organic polymers in visible-light photocatalysis, *J. Mater. Chem. A*, 2020, **8**(15), 7003–7034, DOI: **10.1039/d0ta00364f**.

16 Z. Liu, Q. Su, P. Ju, X. Li, G. Li, Q. Wu and B. Yang, A hydrophilic covalent organic framework for photocatalytic oxidation of benzylamine in water, *Chem. Commun.*, 2020, **56**(5), 766–769, DOI: **10.1039/c9cc07661a**.

17 S. Kim, K. Landfester and C. T. J. Ferguson, Hairy Conjugated Microporous Polymer Nanoparticles Facilitate Heterogeneous Photoredox Catalysis with Solvent-Specific Dispersibility, *ACS Nano*, 2022, **16**(10), 17041–17048, DOI: **10.1021/acsnano.2c07156**.

18 B. A. Marinho, R. O. Cristovao, R. Djellabi, A. Caseiro, S. M. Miranda, J. M. Loureiro, R. A. R. Boaventura, M. M. Dias, J. C. B. Lopes and V. J. P. Vilar, Strategies to reduce mass and photons transfer limitations in heterogeneous photocatalytic processes: Hexavalent chromium reduction studies, *J. Environ. Manage.*, 2018, **217**, 555–564, DOI: **10.1016/j.jenvman.2018.04.003**.

19 M. d. l. M. Ballari, R. Brandi, O. Alfano and A. Cassano, Mass transfer limitations in photocatalytic reactors employing titanium dioxide suspensions, *Chem. Eng. J.*, 2008, **136**(2–3), 242–255, DOI: **10.1016/j.cej.2007.03.031**.

20 A. Chaudhuri, S. D. A. Zondag, J. H. A. Schuurmans, J. van der Schaaf and T. Noel, Scale-Up of a Heterogeneous Photocatalytic Degradation Using a Photochemical Rotor-Stator Spinning Disk Reactor, *Org. Process Res. Dev.*, 2022, **26**(4), 1279–1288, DOI: **10.1021/acs.oprd.2c00012**.

21 R. Li, J. Heuer, T. Kuckhoff, K. Landfester and C. Ferguson, pH-triggered Recovery of Organic Polymer Photocatalytic Particles for the Production of High Value Compounds and Enhanced Recyclability, *Angew. Chem., Int. Ed.*, 2023, e202217652, DOI: **10.1002/anie.202217652**.

22 W. Zhang, H. Shimakoshi, N. Houfuku, X. M. Song and Y. Hisaeda, A polymerized ionic liquid-supported B12 catalyst with a ruthenium trisbipyridine photosensitizer for photocatalytic dechlorination in ionic liquids, *Dalton Trans.*, 2014, **43**(37), 13972–13978, DOI: **10.1039/c4dt01360c**.

23 J. J. Lessard, G. M. Scheutz, A. B. Korpusik, R. A. Olson, C. A. Figg and B. S. Sumerlin, Self-catalyzing photoredox polymerization for recyclable polymer catalysts, *Polym. Chem.*, 2021, **12**(15), 2205–2209, DOI: **10.1039/d1py00208b**.

24 L. Petrizza, M. Le Bechec, E. Decompte, H. El Hadri, S. Lacombe and M. Save, Tuning photosensitized singlet oxygen production from microgels synthesized by polymerization in aqueous dispersed media, *Polym. Chem.*, 2019, **10**(23), 3170–3179, DOI: **10.1039/c9py00157c**.

25 W.-J. Yoo and S. Kobayashi, Efficient visible light-mediated cross-dehydrogenative coupling reactions of tertiary amines catalyzed by a polymer-immobilized iridium-based photocatalyst, *Green Chem.*, 2014, **16**(5), 2438–2442, DOI: **10.1039/c4gc00058g**.

26 J. Heuer, T. Kuckhoff, R. Li, K. Landfester and C. T. J. Ferguson, Tunable Photocatalytic Selectivity by Altering the Active Center Microenvironment of an Organic Polymer Photocatalyst, *ACS Appl. Mater. Interfaces*, 2023, **15**(2), 2891–2900, DOI: **10.1021/acsami.2c17607**.

27 T. Kuckhoff, R. Brewster, C. Ferguson and A. Jarvis, Reactivity Tuning of Metal-Free Artificial Photoenzymes through Binding Site Specific Bioconjugation, *Eur. J. Org. Chem.*, 2023, **26**(e202201412), DOI: **10.1002/ejoc.202201412**.

28 W. Cai, D. Xu, L. Qian, J. Wei, C. Xiao, L. Qian, Z. Y. Lu and S. Cui, Force-Induced Transition of pi-pi Stacking in a Single Polystyrene Chain, *J. Am. Chem. Soc.*, 2019, **141**(24), 9500–9503, DOI: **10.1021/jacs.9b03490**.

29 A. Delgado-Gonzalez, E. Garcia-Fernandez, T. Valero, M. V. Cano-Cortes, M. J. Ruedas-Rama, A. Unciti-Broceta, R. M. Sanchez-Martin, J. J. Diaz-Mochon and A. Orte, Metallofluorescent Nanoparticles for Multimodal Applications, *ACS Omega*, 2018, **3**(1), 144–153, DOI: **10.1021/acsomega.7b01984**.

30 Q. Y. Wu, X. N. Chen, L. S. Wan and Z. K. Xu, Interactions between polyacrylonitrile and solvents: density functional theory study and two-dimensional infrared correlation analysis, *J. Phys. Chem. B*, 2012, **116**(28), 8321–8330, DOI: **10.1021/jp304167f**.

31 Z. Bao, C. Lu, C. Qin, S. Tang, L. Dai, G. Chen and F. Mei, Preparation of fluorescent polyacrylonitrile nanofiber membrane based on polymerizable 1,8-naphthalimide fluorescent disperse dye, *Fibers Polym.*, 2017, **18**(6), 1017–1024, DOI: **10.1007/s12221-017-7053-7**.

32 B. A. DaSilveira Neto, A. S. A. Lopes, G. Ebeling, R. S. Gonçalves, V. E. U. Costa, F. H. Quina and J. Dupont, Photophysical and electrochemical properties of π-extended molecular 2,1,3-benzothiadiazoles, *Tetrahedron*, 2005, **61**(46), 10975–10982, DOI: **10.1016/j.tet.2005.08.093**.

33 M. Grabolle, M. Spieles, V. Lesnyak, N. Gaponik, A. Eychmüller and U. Resch-Genger, Determination of the Fluorescence Quantum Yield of Quantum Dots: Suitable Procedures and Achievable Uncertainties, *Anal. Chem.*, 2009, **81**(15), 6285–6294, DOI: **10.1021/ac900308v**.

34 N. Elgrishi, K. J. Rountree, B. D. McCarthy, E. S. Rountree, T. T. Eisenhart and J. L. Dempsey, A Practical Beginner's Guide to Cyclic Voltammetry, *J. Chem. Educ.*, 2017, **95**(2), 197–206, DOI: **10.1021/acs.jchemed.7b00361**.

35 A. D. Becke, Density–functional thermochemistry. III. The role of exact exchange, *J. Chem. Phys.*, 1993, **98**(7), 5648–5652, DOI: **10.1063/1.464913**.

36 P. J. Stephens, F. J. Devlin, C. F. Chabalowski and M. J. Frisch, Ab Initio Calculation of Vibrational Absorption and Circular Dichroism Spectra Using Density Functional Force Fields, *J. Phys. Chem.*, 1994, **98**(45), 11623–11627, DOI: **10.1021/j100096a001**.

37 G. A. Petersson and M. A. Al-Laham, A complete basis set model chemistry. II. Open–shell systems and the total energies of the first–row atoms, *J. Chem. Phys.*, 1991, **94**(9), 6081–6090, DOI: **10.1063/1.460447**.

38 G. A. Petersson, A. Bennett, T. G. Tensfeldt, M. A. Al–Laham, W. A. Shirley and J. A. Mantzaris, Complete basis

© 2024 The Author(s). Published by the Royal Society of Chemistry

RSC Appl. Polym., 2024, **2**, 155–162 | **161**

set model chemistry. I. The total energies of closed–shell atoms and hydrides of the first–row elements, *J. Chem. Phys.*, 1988, **89**(4), 2193–2218, DOI: **10.1063/1.455064**.

39 N. Huber, R. Li, C. T. J. Ferguson, D. W. Gehrig, C. Ramanan, P. W. M. Blom, K. Landfester and K. A. I. Zhang, A PMMA-based heterogeneous photocatalyst for visible light-promoted [4 + 2] cycloaddition, *Catal. Sci. Technol.*, 2020, **10**(7), 2092–2099, DOI: **10.1039/d0cy00016g**.

40 T. Kuckhoff, K. Landfester, K. A. I. Zhang and C. T. J. Ferguson, Photocatalytic Hydrogels with a High Transmission Polymer Network for Pollutant Remediation, *Chem. Mater.*, 2021, **33**(23), 9131–9138, DOI: **10.1021/acs.chemmater.1c02180**.

41 P. Makula, M. Pacia and W. Macyk, How To Correctly Determine the Band Gap Energy of Modified Semiconductor Photocatalysts Based on UV-Vis Spectra, *J. Phys. Chem. Lett.*, 2018, **9**(23), 6814–6817, DOI: **10.1021/acs.jpclett.8b02892**.

42 J. Tauc, R. Grigorovici and A. Vancu, Optical Properties and Electronic Structure of Amorphous Germanium, *Phys. Status Solidi B*, 1966, **15**(2), 627–637, DOI: **10.1002/pssb.19660150224**.

43 M. H. Gehlen, The centenary of the Stern-Volmer equation of fluorescence quenching: From the single line plot to the SV quenching map, *J. Photochem. Photobiol., C*, 2020, **42**, 100338, DOI: **10.1016/j.jphotochemrev.2019.100338**.

44 Y. Q. Zou, J. R. Chen, X. P. Liu, L. Q. Lu, R. L. Davis, K. A. Jorgensen and W. J. Xiao, Highly efficient aerobic oxidative hydroxylation of arylboronic acids: photoredox catalysis using visible light, *Angew. Chem., Int. Ed.*, 2012, **51**(3), 784–788, DOI: **10.1002/anie.201107028**.

45 S. P. Pitre, C. D. McTiernan, H. Ismaili and J. C. Scaiano, Mechanistic insights and kinetic analysis for the oxidative hydroxylation of arylboronic acids by visible light photoredox catalysis: a metal-free alternative, *J. Am. Chem. Soc.*, 2013, **135**(36), 13286–13289, DOI: **10.1021/ja406311g**.

46 R. Li, *Visible light-induced organic transformations using benzothiadiazole derivates as highly efficient photocatalysts*, phd, Johannes Gutenberg-Universität, Mainz, 2017. **https://hdl.handle.net/21.11116/0000-0000-B34B-2**.

47 Y. Li, P. Ren, D. Zhang, W. Qiao, D. Wang, X. Yang, X. Wen, M. H. Rummeli, H. Niemantsverdriet, J. P. Lewis, *et al.*, Rationally Designed Metal Cocatalyst for Selective Photosynthesis of Bibenzyls via Dehalogenative C–C Homocoupling, *ACS Catal.*, 2021, **11**(7), 4338–4348, DOI: **10.1021/acscatal.1c00102**.